2023 45th Annual International Conference of the IEEE Engineering in Medicine & Biology Society (EMBC) | 979-8-3503-2447-1/23/$31.00 ©2023 IEEE | DOI: 10.1109/EMBC40787.2023.10340550

A Surface-Integrated Sensor Network for Personalized Multifunctional Catheters*

Nishant Gupta[1,2], Gerhard Kuert[1], Adrian Ryser[3], Andreas Haeberlin[3] and Thomas Niederhauser[1,2], *Member, IEEE*

***Abstract*— Augmenting the sensing/actuating capabilities of multifunctional catheters used for minimally invasive interventions has been fostered by the reduction of transducers' sizes. However, increasing the number of transducers to benefit from the entire catheter surface is challenging due to the number of connections and/or the required integrated circuits dedicated for multiplexing the transducer signals. Modular concepts enabling personalized catheters are lacking, at all. In this work, we investigated the feasibility of a simple and daisy-chainable transducer node network for active catheters, which overcomes these limitations. Sequentially accessible nodes enabling analog interaction (including signal buffering) with transducers were designed and fabricated using miniature components suited for catheter integration. The effective sampling rate (ESR) per node for acquiring bio-signals from 10 nodes was examined for various signal-to-noise ratios. Thanks to the low circuit complexity, an ESR up to 20 kHz was achieved, which is high enough for many bio-signals.**

***Clinical relevance*— Typical daisy-chaining features, namely theoretically indefinite node extension and simple reconfiguration facilitates modularization of the catheter design. The proposed network consequently ensures application and patient-specific requirements while incorporating transducer functions over the entire catheter surface, both may improve minimally invasive interventions.**

I. Introduction

Continued progress of miniature transducers, integrated-circuits (ICs) and flexible substrates have opened new possibilities for minimally-invasive interventions and implantable medical devices. Consequently, catheter-based diagnosis and treatments have gained much attention towards adding intra-corporeal sensing and actuating capabilities that benefit from improved tissue interaction compared to extra-corporeal transducers [1], [2]. By creating multiple sensor/actuation nodes along the catheter surface, multiple internal body regions can potentially be targeted simultaneously. However, incorporating several transducers together with the required wiring in catheters is cumbersome due to the stringent space and flexibility constraints. Another challenge with multi-site monitoring is that the optimal distances between the sensing regions may be patient specific (such as age, gender, and organ size). Furthermore, the optimal combination of sensing modalities and their number would vary with application requirements. Hence, a modular approach adaptable to different scenarios is of high interest.

*This work was funded by the SNSF (20B1-1_186321/1) and by the Swiss Innovation Agency - Innosuisse (56257.1 IP-LS).

[1]Nishant Gupta, Gerhard Kuert, Adrian Ryser and Thomas Niederhauser are with the Institute for Human Centred Engineering, Bern University of Applied Sciences, Biel, Switzerland (e-mail: {nishant.gupta, thomas.niederhauser}@bfh.ch)

[2]Nishant Gupta and Thomas Niederhauser are also with the sitem Center for Translational Medicine and Biomedical Entrepreneurship, Bern, Switzerland

[3]Adrian Ryser and Andreas Haeberlin are with the Department of Cardiology, Inselspital, Bern University Hospital, Bern, Switzerland

(a)

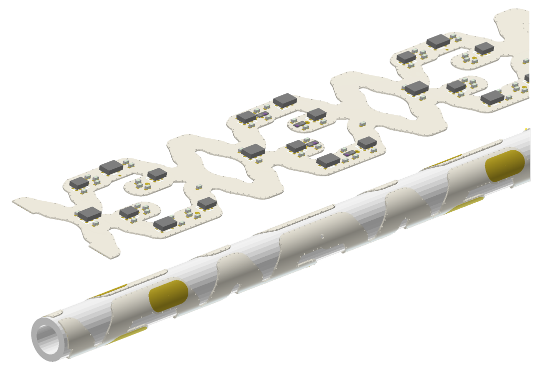

(b)

Fig. 1: Conceptual design of a smart catheter using (a) a flexible printed circuit board with assembled ICs (b) wrapped around a polymer tube.

Existing networking topologies for multi-sensor catheters use either a central multiplexer or a grid-based distributed multiplexer [3], both lacking scalability. The central multiplexer is restricted by the connection congestion and size bottlenecks. The grid-based approach addresses these issues but requires multiple row/column selecting signals, thus reducing the available sensor connections. Modular sensor networks are commonly used in industrial control systems, but the typical communication protocols (CAN, LIN, I^2C, etc.) require signal digitization and complex processing at each node, thus are not suited for size-constrained catheters.

We investigated the feasibility of integrating a network of multiplexed transducers into the catheter surface. A modified distributed multiplexing approach for analog signals to allow addressing the nodes sequentially was used. Catheter prototypes were fabricated using a novel technique [4] in which medical-grade tubes are laminated with flexible printed circuit boards (FPCBs) integrating the transducers nodes. Mechanical characteristics of the prototypes as well as the effective sampling rate (ESR) achievable per node were studied. We also compared the latter with 'directly addressed' networks for commonly acquired bio-signals.

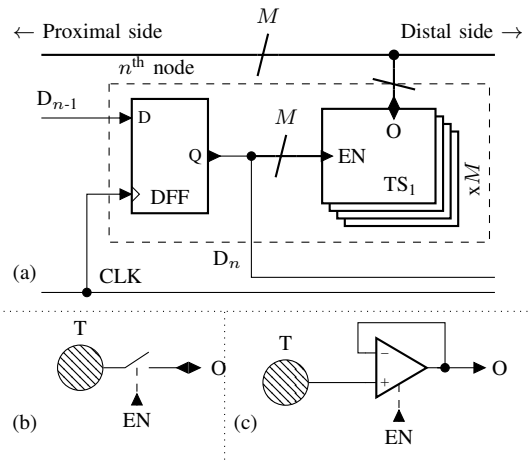

Fig. 2: (a) Principal circuit of a node. (b) Bi-directional transducer-switch (TS) interface. (c) Buffered TS interface

II. Materials and methods

A. Catheter prototypes

The catheter prototypes were fabricated starting from a liquid crystal polymer (LCP) based multi-layer FPCB. The transducers and ICs were attached to the FPCB using standard surface mounting techniques (Fig. 1 (a)). The FPCB was subsequently laminated via thermo-bonding onto a flexible thermoplastic poly urethane (TPU) tube having an outer diameter of 3mm (Fig. 1 (b)). All the components were placed on the inner FPCB surface in order to encapsulate them between the FPCB and the TPU tube. Physical stress arising on the components due to catheter bending was minimized by orienting each component along the catheter axis. Each node contained up to four transducers to capture biosignals from each direction. The outer FPCB layer contained electrodes and apertures to connect the acquired biosignals to the inner components, while the internal layers were used for the circuit design. Post lamination, radial cross sections were prepared to visually analyze the component's encapsulation.

B. Daisy-chainable nodes and sequential addressing

Fig. 2(a) illustrates the node circuit, in which the sequentially connected D-type flip-flops (DFF) of N nodes provide access to the individual node. Node selection is performed by clocking a one-hot (D_0 is high before the $[N-n+1]^{\text{th}}$ CLK only) bit pattern of length N via D_0 in the most proximal node. The output of the target DFF (D_n) enables all the M transducer-switch (TS) interfaces in the node (via EN input) and also connects to the next node in the chain. By repeating this process for each n, all $M \times N$ transducers are interfaced using only $O(M)+2$ connections. Once connected, interaction (activation/measurement) with all M TS interfaces can be performed by a proximally or externally located hub.

For the TS interface, we considered two variants: 1) direct connection via an 'analog switch' (TS_1, Fig. 2 (b)), and 2) buffered connection using a 'multiplexable op-amp' (TS_2, Fig. 2 (c)). While TS_1 provides fast bi-directional access to the transducers, TS_2 reduces the susceptibility of the measured signal towards external noise and interference.

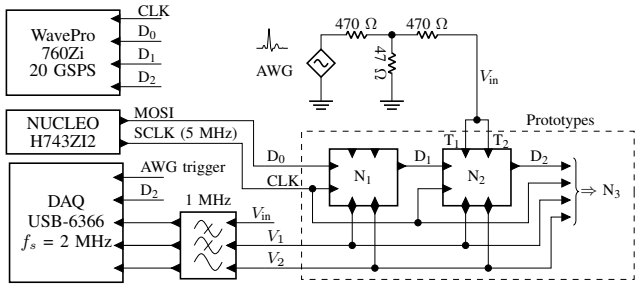

Fig. 3: Test-setup used to characterize the node network.

C. Test setup for the network characteristics

Fig. 3 describes the setup used to test and analyze the network characteristics. The D_0 and CLK signals were generated using the serial parallel interface (SPI: MOSI and SCLK) of an ARM microcontroller board (STM32 Nucleo H743ZI2). The SPI CLK time period (t_{CLK}) and the length N were directly programmed in the firmware and the node location (n) was communicated via the USB serial port.

In order to minimize the transducer related noise and signal interference, an arbitrary waveform generator (AWG) (81150A, Agilent Technologies) in series with a resistor network was used to simulate the transducer signal. A known electrocardiogram (ECG) at 120 beats/minute (2 Hz) signal was generated and attenuated to obtain a 9 mV (plus 0.81 V offset) signal. Both the transducer-switch interfaces (TS_1 and TS_2) of the bio-potential node (N_2) were supplied with the identical V_{in}. Since other bio-signals, such as pressure, photoplethysmography (PPG) and temperature, have typically lower bandwidth requirements compared to ECG signals, testing only with an ECG sequence was deemed sufficient for analyzing the network characteristics.

The input signal (V_{in}) and the voltage on the shared I/O lines of the two TS interfaces (V_m where $m \in \{1,2\}$), were recorded using a 16-bit data acquisition system (DAQ, National Instruments USB-6366) at f_s = 2 mega samples per second (MSPS) rate. The analog inputs were bandwidth restricted (-3 dB at 1 MHz) using a first-order low-pass filter. A weak pull-down to the ground using 100 kΩ was applied to prevent floating inputs. The D_2 output and the AWG trigger for the ECG signal were also recorded using the DAQ for time synchronization. CLK and $D_{0,1,2}$ signals were captured separately using a 20 GSPS oscilloscope (WavePro 760Zi, Teledyne Lecroy) triggered with the rising edge of the first CLK pulse to measure the communication time.

For the data acquisition, a script to interface the microcontroller, the AWG, and the DAQ was written in Matlab (R2020b, Mathworks Inc.). All the switches were initialized to the off state. Data was recorded for 5 seconds after starting the ECG signal generation with N_2 being activated at around

1-second mark. The D_2 rising edge was used to set $t = 0$ for all signals.

D. Effective sampling rate (ESR)

For multiplexed data measurements the ESR (per node) can be defined as:

$$\text{ESR} = 1/\left(Nt_t\right) = 1/\left(N\left(t_c + t_s + t_a\right)\right) \tag{1}$$

where t_t is the total time spent at each node n. The three sub-components t_c, t_s, and t_a are the communication, settling, and acquisition time, respectively.

For the proposed network, t_c is $N \times t_{\text{CLK}}$ in the worst case scenario of random node access. In strictly sequential mode t_c can be reduced to t_{CLK}, however, this may not be optimal in multi-modal scenarios. For 'directly addressed' networks (such as multiplexers or grid-based row/column selects), t_c is generally limited by the logic gates and transmission delays and typically only a few nanoseconds. Hence, we consider them negligible comparing with the proposed approach.

The settling time t_s is the time taken from node activation (t = 0) until the moving mean absolute difference (MMAD) of V_{m} and V_{in} falls below a certain threshold. To avoid the influence of random fluctuations, a ($2K$+1)-point central average was used for to estimate MMAD:

$$\text{MMAD}_{\text{m}}[t] = \frac{1}{2K+1}\sum_{k=-K}^{K}\left|(V_{\text{m}} - V_{\text{in}})[t + k/f_s]\right| \tag{2}$$

MMAD was chosen such that typical error sources before V_{in} (such as resistance mismatch, AWG gain and offset errors, and environmental noise) do not influence t_s. The odd-point central average does not introduce an additional delay, as well. For the current setup, we used K = 1 and the MMAD threshold was set to 2 mV.

The acquisition time t_a was defined as the sampling time for achieving an acceptable signal-to-error ratio (SER). The 'error' was defined for the three measurements ($V = \{V_{\text{in}}, V_1, V_2\}$) based on their difference from the 'true' signal V_{ECG} after some settling time (t'_s) set *a-priori*. V_{ECG} was determined from the AWG settings, the voltage divider configuration and the recorded synchronization signals. SER was calculated for multiple t_a using signal decimation. Hence, the SER calculates to:

$$\text{SER}[t_a] = \frac{\sigma^2\left(V_{\text{ECG},t_a\times f_s\downarrow}[t > t'_s]\right)}{\sigma^2\left((V - V_{\text{ECG}})_{t_a\times f_s\downarrow}[t > t'_s\right)}, \tag{3}$$

where the subscript $t_a \times f_s \downarrow$ denotes the decimation factor and t'_s was set to 1 ms post node selection.

III. Results

Figure 4 shows a zoomed view of the cross-section of a fabricated catheter prototype. Both, the capacitor and the IC as part of one node are completely encapsulated in the TPU tube bonded to the innermost LCP layer. The maximal outer diameter of the catheter section and the wall thickness were measured as 3.3 mm and 0.55 mm, respectively.

The analog signals recorded by the DAQ are shown in Fig. 5 (a). As expected, V_1 and V_2 transition from ∼0 V to V_{in} at node selection (t = 0). The t_c determined from the communication signals (Fig. 5 (b)), was measured to be 1.8 µs, which is in line with the calculated 2 µs (= $N \times t_{\text{CLK}}$) considering that 1 clock cycle (t_{CLK} = 200 ns) is required by the sequential logic for setting the D_0 prior to the first SPI CLK edge. Slightly increased ringing in D_1 and D_2 compared to D_0 can be observed as well.

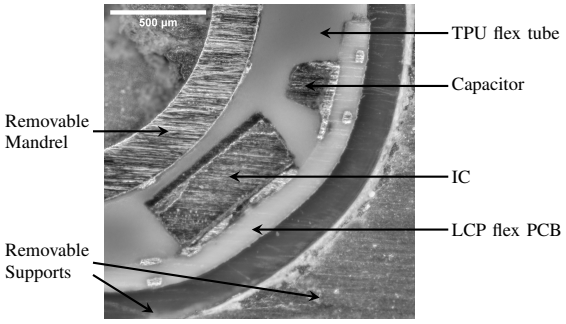

Fig. 4: Wall cross-section of a catheter prototype.

Estimation of the MMAD just after D_2 rising edge (t = 0) are depicted in Fig. 6 as a function of t_s for the two interfaces. For TS_1, $1/t_s$ = 400 kHz is close to the bandwidth of the current setup (1 MHz), hence could be limited by the latter. For TS_2, t_s = 138.5 µs is in line with the settling behavior of the op-amp as illustrated in the data sheet [5].

SER[t_a] was found nearly identical for the three signals $V = \{V_{\text{in}}, V_1, V_2\}$ (Fig. 7). The std error $\sigma(V - V_{\text{ECG}})$ and (SER[0.5 µs]) were also similar at 700 µV (7.36 dB), 704 µV (7.32 dB), 706 µV (7.40 dB) for V_{in}, V_1, and V_2, respectively. These results suggest that neither TS_1 nor TS_2 adds significant noise to the signal, and the same t_a can be applicable for both. Beyond t_a = 110 µs (20.83 dB) the SER improvement starts to converge at SER[2 ms] = 21.75 dB.

To finally estimate ESR using (1), we considered the extreme values for t_s (2.5 µs to 138.5 µs, Fig. 6) and t_a (0.5 µs to 110 µs, Fig. 7). For the proposed network, the ESR was estimated at t_c = 2 µs for N = 10 and ranged from 400 Hz to ∼20 kHz. For directly addressed nodes, ESR was estimated by ignoring t_c and ranged between ∼402 Hz and ∼33 kHz, for the same t_s, t_a, and N.

IV. Discussion

The proposed topology offers key benefits to realize a modular active transducer network in space-constrained catheters. Whereas central and grid-based multiplexing require $O(M \times N)$ and $O(M + N)$ connections, respectively, the proposed network requires $O(M)+2$ connections, only. The low connection density, which is independent on the number of nodes N, enables daisy-chaining, i.e. the possibility to add nodes without adding signals for addressing them and also reduces signal interferences due to channel cross-talk or track impedances. Moreover, the nodes can be designed as interchangeable modules, allowing their ordering, number and density to be re-configured based on application- and patient-specific needs. Integrating the

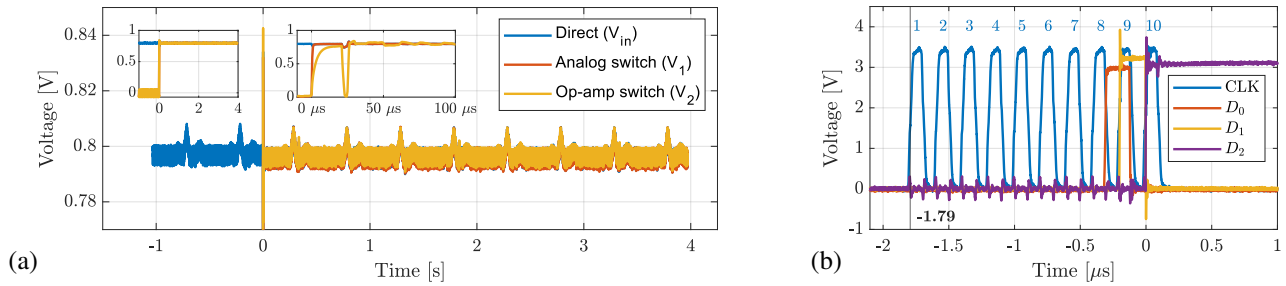

Fig. 5: (a) Raw analog signals. (Inset left) Full view on the voltage scale. (Inset right) Zoomed in around the transition. (b) Communication signal for selecting the 2nd node.

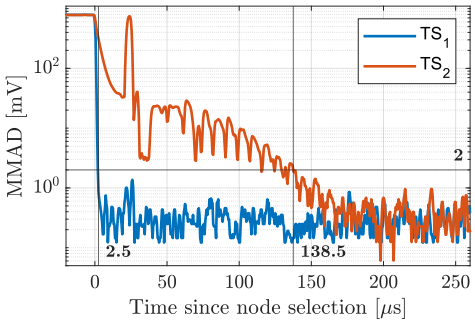

Fig. 6: Estimation of t_s for the two interfaces based on the moving average absolute difference (MMAD)

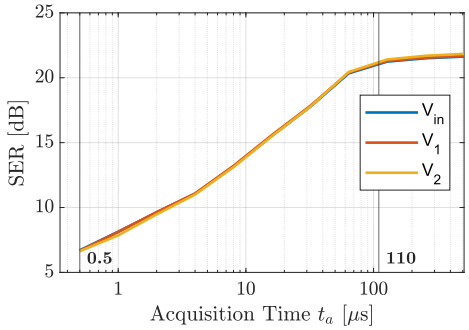

Fig. 7: Signal to error ratio (SER) dependence on t_a

the complete functionality (transducers, associated ICs and connections) in the wall simplifies the design of catheters providing outstanding sensing functionality while ensuring the catheter lumen to be used e.g for liquid transport or guide-wire access.

This work shows that such a daisy-chained sensor network is feasible. Basic visual analysis show that complete encapsulation of the components was possible while achieving an outer catheter diameter of 3.3 mm and 0.55 mm wall thickness. These dimensions should be suitable to access tubular organs such as the esophagus, the trachea, and the major arteries and veins in adults. Further reduction might be required to cope with more demanding applications (smaller pathways) and age groups (children and neonates). Continued improvements in integrated fabrication processes for flexible sensors and electronics might pave this way [6], [7].

Further studies in living subjects are planned, which would help evaluating the clinical benefits of a modularized multi-sensor catheter and comparison with existing monitoring methods. For this, a custom measurement setup capable of high-speed multiplexing/de-multiplexing of common bio-signals is currently under development. Efficacy of the proposed circuit in carrying the analog signals from the transducers also needs to be individually validated for each modality. Extremely sensitive signals, such as EMG or pressure, could require additional analog processing beyond signal buffers. Converting such sensor signals to differential signals, for example, may provide further immunity to intracorporeal or external interference.

V. Conclusion

Daisy-chained networks simplify multifunctional catheter design by reducing size constraints associated with conventional networking approaches. Significant reduction in external connection count and simple structural layout is achieved with low impact on the sampling rate that cope with bandwidths of commonly acquired bio-signals. In the future, low-cost design and manufacturing of advanced and personalized catheters using standard electronic components and fabrication methods may become possible.

References

[1] W. Lu *et al.*, "Wireless, implantable catheter-type oximeter designed for cardiac oxygen saturation," *Sci. Adv.*, vol. 7, no. 7, p. eabe0579., Feb. 2021.

[2] T. Sharma, K. Aroom, S. Naik, B. Gill, and J. X. J. Zhang, "Flexible Thin-Film PVDF-TrFE Based Pressure Sensor for Smart Catheter Applications," *Ann. Biomed. Eng.*, vol. 41, no. 4, pp. 744–751, Apr. 2013.

[3] S. P. Lee *et al.*, "Catheter-Based Systems With Integrated Stretchable Sensors and Conductors in Cardiac Electrophysiology," *Proc. IEEE*, vol. 103, no. 4, pp. 682–689, Apr. 2015.

[4] G. Kuert, M. Jacomet, and T. Niederhauser, "Efficient Thermobonding Process Forming a Polyurethane Based Diagnostic Catheter with Liquid Crystal Polymer," *Annu. Int. Conf. IEEE Eng. Med. Biol. Soc.*, vol. 2019, pp. 6163–6166, Jul. 2019.

[5] *Precision, Low-Power and Low-Noise Op Amp with RRIO*, Maxim Integrated Std. MAX40 100, 2 2021, rev. 5.

[6] F. Barz, V. Trouillet, O. Paul, and P. Ruther, "CMOS-Compatible, Flexible, Intracortical Neural Probes," *IEEE Trans. Biomed. Eng.*, vol. 67, no. 5, pp. 1366–1376, Aug. 2019.

[7] Y. Bonnassieux *et al.*, "The 2021 flexible and printed electronics roadmap," *Flexible Printed Electron.*, vol. 6, no. 2, p. 023001, May 2021.